Printed Assemblies of Inorganic Light-Emitting Diodes for Deformable and Semitransparent Displays

Sang-Il Park,[1*] Yujie Xiong,[1*†] Rak-Hwan Kim,[1*] Paulius Elvikis,[2] Matthew Meitl,[3] Dae-Hyeong Kim,[1] Jian Wu,[4] Jongseung Yoon,[1] Chang-Jae Yu,[1] Zhuangjian Liu,[5] Yonggang Huang,[4,6] Keh-chih Hwang,[7] Placid Ferreira,[2] Xiuling Li,[8] Kent Choquette,[8] John A. Rogers[1,2‡]

We have developed methods for creating microscale inorganic light-emitting diodes (LEDs) and for assembling and interconnecting them into unusual display and lighting systems. The LEDs use specialized epitaxial semiconductor layers that allow delineation and release of large collections of ultrathin devices. Diverse shapes are possible, with dimensions from micrometers to millimeters, in either flat or "wavy" configurations. Printing-based assembly methods can deposit these devices on substrates of glass, plastic, or rubber, in arbitrary spatial layouts and over areas that can be much larger than those of the growth wafer. The thin geometries of these LEDs enable them to be interconnected by conventional planar processing techniques. Displays, lighting elements, and related systems formed in this manner can offer interesting mechanical and optical properties.

Display devices represent ubiquitous, central components of nearly all consumer electronics technologies. Organic light-emitting diodes (OLEDs) are rapidly emerging as an attractive alternative to backlit liquid crystals due to their comparatively high refresh rates, contrast ratios, power efficiencies, and capacity for vibrant color rendering (*1*, *2*). Inorganic light-emitting diodes (ILEDs) can also form displays, with properties such as brightness, lifetime, and efficiency that can exceed those possible with OLEDs (*3*, *4*). These displays exist, however, only in ultralarge-area, low-resolution formats (square meters; billboard displays), limited by processing and assembly procedures that do not scale effectively to small (< ~200 μm by 200 μm), thin (< ~200 μm) light emitters or to dense, high–pixel count arrays. An ability to replace existing

[1]Departments of Materials Science and Engineering, Beckman Institute, and Frederick Seitz Materials Research Laboratory, University of Illinois at Urbana-Champaign, 1304 West Green Street, Urbana, IL 61801, USA. [2]Department of Mechanical Science and Engineering, University of Illinois at Urbana-Champaign, 1206 West Green Street, Urbana, IL 61801, USA. [3]Semprius, Durham, NC 27713, USA. [4]Department of Civil and Environmental Engineering, Northwestern University, Evanston, IL 60208, USA. [5]Institute of High Performance Computing, 1 Fusionopolis Way, 16-16 Connexis, Singapore 138632. [6]Department of Mechanical Engineering, Northwestern University, Evanston, IL 60208, USA. [7]Department of Engineering Mechanics, Tsinghua University, Beijing 100084, China. [8]Department of Electrical and Computer Engineering, University of Illinois at Urbana-Champaign, 1206 West Green Street, Urbana, IL 61801, USA.

*These authors contributed equally to this work.
†Present address: School of Engineering and Applied Science, Washington University, St. Louis, MO 63130, USA.
‡To whom correspondence should be addressed. E-mail: jrogers@uiuc.edu

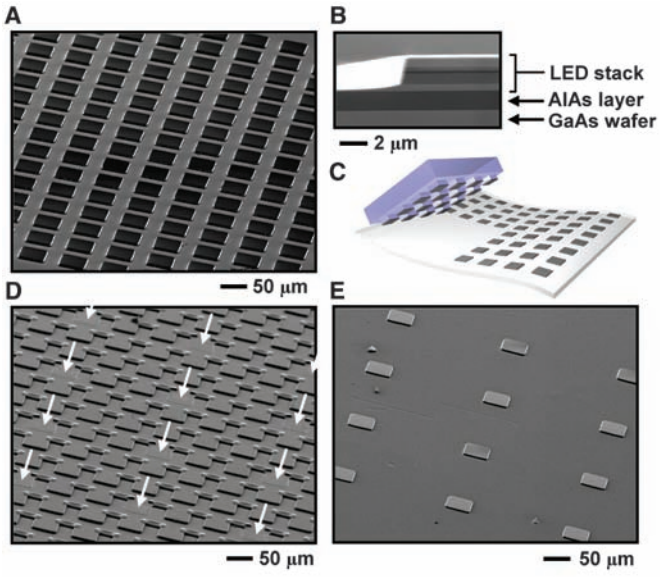

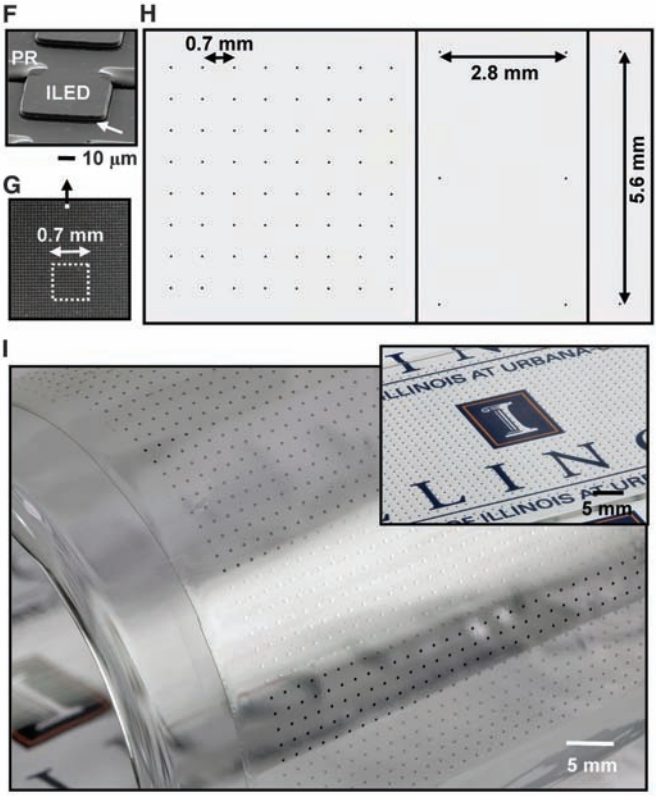

Fig. 1. (**A**) SEM image of a square array of AlInGaP LED structures (50 μm by 50 μm) created by vertical, patterned etching through an epitaxial multilayer stack grown on a GaAs wafer. (**B**) Cross-sectional SEM view of one of these structures, showing the LED semiconductor layers (quantum wells, as well as cladding, spreading, and contact layers) on a sacrificial epilayer of AlAs. (**C**) Schematic illustration of a printing-based assembly method for transferring collections of LEDs (gray) released from the GaAs wafer to a target substrate (shown here as a flexible sheet). (**D**) SEM image of the GaAs wafer after removing a set of LEDs (indicated by white arrows) with a stamp. (**E**) SEM image of a region of the target substrate printed with this stamp. (**F**) Angled-view SEM image of an individual LED (i.e., ILED) from the array in (D). A pair of "breakaway" photoresist (PR) anchors at the two far corners of the device holds it above the GaAs wafer in the suspended configuration of a diving board, for ease of liftoff with a stamp. The white arrow points to the region of removed AlAs. (**G**) SEM image of a dense collection of such devices on a piece of a GaAs wafer. The black arrow and white dot indicate, roughly, the region of this chip that corresponds to the image of (F). (**H**) Optical image of a target substrate printed with sparse arrays of devices at different spacings, derived from the chip shown in (G). (**I**) Large-scale collection of ILEDs (1600 devices, in a square array with pitch of 1.4 mm) printed onto a thin, flexible sheet of plastic, shown here wrapped onto a cylindrical glass substrate (main panel). The inset shows a similar collection of ILEDs (1600 devices, in a square array with pitch of 1.4 mm) printed onto a plate of glass. For these cases, relatively large ILEDs were selected for ease of viewing; devices with dimensions of (E) are invisible at this magnification.

methods for fabricating ILEDs (i.e., wafer sawing, serial pick-and-place, wire bonding, and packaging on a device-by-device basis) and for incorporating them into displays (i.e., robotic assembly into tiles followed by interconnection using large quantities of bulk wiring) with those that more closely resemble the planar, batch processing of OLEDs would greatly expand the application opportunities. Examples include not only ILED displays for desktop monitors, home theater systems, and instrumentation gauging, but also, when implemented in flexible or stretchable forms, wearable health monitors or diagnostics and biomedical imaging devices. In microscale sizes, such ILEDs can also yield semitransparent displays, with the potential for bidirectional emission characteristics, for vehicle navigation, heads-up displays, and related uses.

We present routes to create ultrathin, ultrasmall ILEDs in flat or "wavy" geometries and to assemble them into addressable arrays using scalable processing techniques, on substrates ranging from glass to plastic and rubber. The strategy involves four key components: (i) epitaxial semiconductor multilayers designed for lateral delineation and release from a source wafer to yield isolated arrays of ILEDs, each of which remains tethered to the wafer by polymeric "breakaway" anchor structures; (ii) printing techniques for manipulating the resulting ILEDs in schemes that enable formation of large-scale arrays on foreign substrates and in arbitrary spatial layouts; (iii) planar processing methods for establishing electrical interconnects to the devices, in direct or matrix addressable configurations; and (iv) integration strategies capable of yielding ILED displays in flexible or stretchable formats and with conventional, semitransparent, or bidirectional emission characteristics. Certain aspects build on previously reported procedures for etching and manipulating epitaxial semiconductor layers (*5*–*11*) and for fabricating flexible and stretchable electronics (*12*, *13*).

Figure 1 presents essential aspects of the first two of the components [see supporting online material (SOM) for details]. The epitaxial semiconductor layers include AlInGaP quantum well structures (6-nm-thick $In_{0.56}Ga_{0.44}P$ wells, with 6-nm-thick barriers of $Al_{0.25}Ga_{0.25}In_{0.5}P$ on top and bottom), cladding films (200-nm-thick layers of $In_{0.5}Al_{0.5}P$:Zn and $In_{0.5}Al_{0.5}P$:Si for the p and n sides, respectively), spreaders (800-nm-thick layers of $Al_{0.45}Ga_{0.55}As$:C and $Al_{0.45}Ga_{0.55}As$:Si for the p and n sides, respectively), and contacts (5-nm-thick layer of GaAs:C and 500-nm-thick layer of GaAs:Si for the p and n sides, respectively), for a total thickness of ~2.523 μm, all grown on AlAs (1500-nm-thick layer of $Al_{0.96}Ga_{0.04}As$:Si) on a GaAs substrate (fig. S1). The AlAs can be removed by etching with hydrofluoric (HF) acid, in procedures that do not alter the overlying layers or the underlying substrate. The process for defining the ILEDs first involves forming a pattern of vertical trenches through the epitaxial layers by inductively coupled plasma reactive ion etching through a mask of SiO_2 defined photolithographically (fig. S2). This step determines the lateral geometries of the devices (fig. S2). Figure 1, A and B, shows top and cross-sectional scanning electron microscope (SEM) images collected after this etching process for a representative case, where the device islands in Fig. 1 are 50 μm by 50 μm. Creating a pattern of photoresist posts (i.e., "breakaway" anchors) located at two of the four corners of each island, followed by immersion in concentrated HF, leads to the undercut release of an organized array of ILEDs. The anchors hold the devices in their lithographically defined locations to prevent lift-off into the etching bath, even after complete undercut (fig. S2). Next, an automated printing tool (fig. S3) brings a soft elastomeric stamp with features of relief embossed onto its surface into aligned contact with a selected set of these ILEDs. Peeling the stamp away fractures the photoresist anchors and leaves the devices adhered via Van der Waals interactions to the raised regions of relief. Figure 1, C and D, shows schematic illustrations of the printing process and an SEM image of an array of anchored ILEDs on the source wafer after one cycle of printing (fig. S4). The white arrows in Fig. 1D highlight the collection of ILEDs removed by this process, corresponding to every third device along the two orthogonal axes of the square array. Figure 1E provides an SEM image of these devices printed onto a glass substrate. The engineering design of the breakaway anchors is such that they are sufficiently robust to hold the ILEDs in their

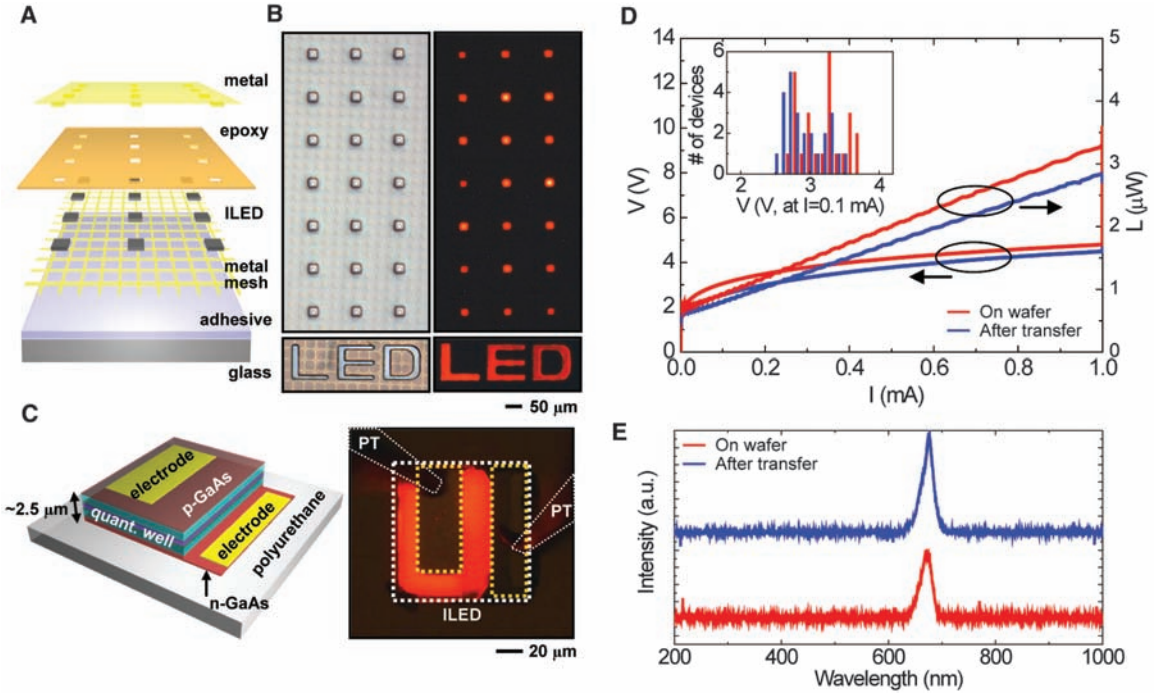

Fig. 2. (**A**) Exploded view schematic illustration of an array of ILEDs contacted by a metal mesh (bottom; n contacts) and a metal film (top; p contacts). A thin adhesive layer of PDMS facilitates printing onto the glass substrate. A photopatterned layer of epoxy on top of the devices prevents shorting of the top film to the bottom mesh. (**B**) Optical micrographs of an array of ILEDs (top: 25 μm by 25 μm, square geometries; bottom: characters "LED") in their off state with frontside illumination (left) and in their on state without illumination (right). (**C**) Schematic illustration of an ILED with integrated ohmic contacts (left) and optical image of an operating device (right), showing uniform emission characteristics at all regions not directly blocked by the contacts or probe tips. The areas delineated by yellow and white dashed boxes correspond to the contact electrodes and the device periphery, respectively. The regions labeled "PT" correspond to the probe tips used to evaluate the device operation. (**D**) Current-voltage-emission characteristics of a representative device before undercut etching on the GaAs wafer, and after transfer printing onto a polyurethane-coated glass slide. The inset provides a histogram of the bias voltages needed to produce currents of 0.1 mA in a collection of devices. (**E**) Spectral characteristics of emission for a typical device on the wafer and after transfer printing.

lithographically defined locations during the undercut etching and drying processes but sufficiently fragile to enable high-yield liftoff during printing. Three key design aspects are the use of (i) a pair of anchors on the same side of each ILED, to yield, after undercut, suspended, "diving board" layouts (Fig. 1F) that enable transfer of torques large enough to fracture the photoresist upon peel-back of the stamp; (ii) stamps with relief structures that are slightly smaller than the ILEDs and are offset from the centers of the devices to maximize these torques and also to minimize overlap with the anchors; and (iii) photoresist structures that fracture more readily than the semiconductor material. This type of anchoring scheme (i.e., heterogeneous anchoring) is much more efficient in active materials utilization and versatile in design choices than corresponding methods demonstrated previously for transistors (*12*) and solar cells (*14*), where peripheral parts of the devices themselves serve as the anchors (i.e., homogeneous anchoring). Conventional wafer dicing and pick-and-place methods are not suitable for devices with the thicknesses and dimensions in the range reported here, due to challenges associated with wafer utilization, device fragility, and size. Such techniques also lack the high-throughput, parallel operation of the type of printing methods described above.

Figure 1G shows a micrograph of a densely packed array of anchored, undercut ILEDs on a source wafer. Figure 1H shows sparse assemblies of these devices formed by printing in a step-and-repeat fashion from this wafer to a glass substrate, coated with a thin (~10 μm) layer of poly(dimethylsiloxane) (PDMS) to promote dry, conformal adhesion (details are in the SOM). As examples of high yields, large areas, and compatibility with plastic substrates, Fig. 1I presents images of collections of ILEDs printed onto a thin sheet of polyethylene terephthalate (PET, 50 μm thick), shown as wrapped around a cylindrical glass support (1600 devices, in a square array with pitch of 1.4 mm; radius of cylinder ~25 mm) and onto a plate of glass (inset; 1600 devices, in a square array with pitch of 1.4 mm). The overall fabrication yields, including delineation and undercut of the ILEDs and subsequent printing of them onto the target substrates, were 100% in both cases. The devices were selected to have sizes (i.e., 250 μm by 250 μm) large enough to be visible in the images; those with sizes of Fig. 1D are too small to be seen clearly at these scales.

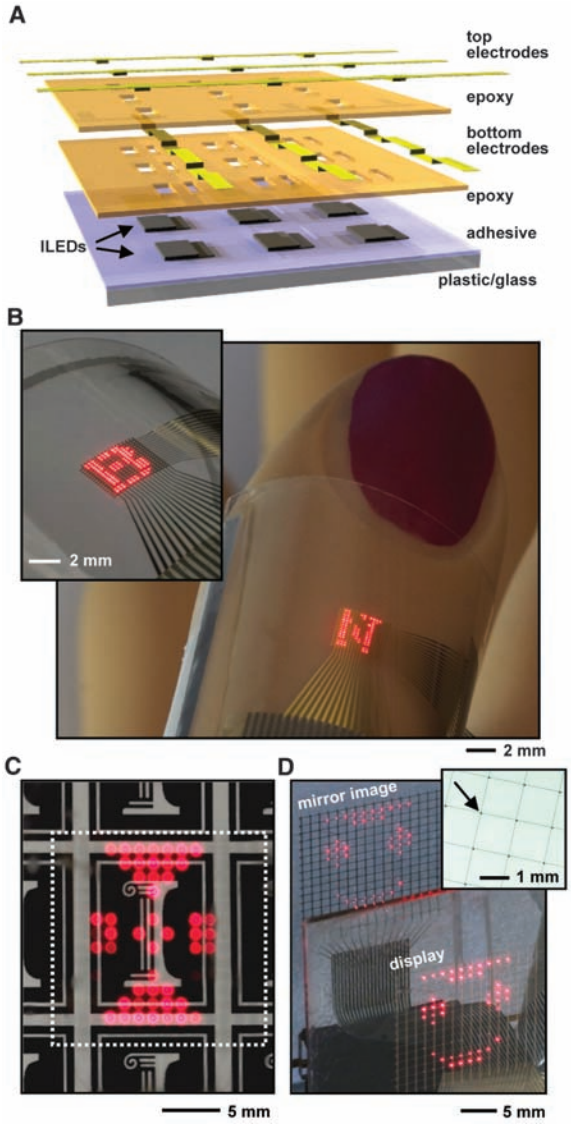

Fig. 3. (**A**) Schematic illustration of a planar scheme for interconnecting a printed array of ILEDs in a passive matrix layout. Coordinated control of voltages applied to the row and column electrodes allows operation in a passive matrix display mode. (**B**) Images of a flexible display that incorporates a 16 by 16 array of ILEDs in the layout shown in (A), on a sheet of plastic (PET), wrapped around the thumb of a mannequin hand (main panel; human scale; radius ~8 mm) and a cylindrical glass tube (inset; radius ~12 mm). External interface to control electronics occurs through ribbon cables bonded to column and row electrodes that emerge from the periphery of the display. (**C**) Image of a comparatively large, semitransparent display that uses a similar layout but with a sparse array of ILEDs on a glass substrate. The camera is focused on the paper in the background; the white dashed box illustrates the perimeter of the active region of the display. (**D**) Image of a similar device (bottom right) displaying a different pattern in front of a mirror (upper left), to illustrate the bidirectional emission property. In this system, the ILEDs represent only ~0.8% of the total area. The inset shows a magnified view of a region of the display in its off state, to illustrate the small areal coverage of the devices. The black arrow points to one of the ILEDs, which is barely visible at this magnification.

Establishing electrical connections to these printed ILEDs yields lighting elements or addressable displays. The small thickness (~2.5 μm) of the devices enables the use of conventional thin-film processing, thereby providing a route to displays and related devices that is simpler, more scalable, and applicable to much smaller pixel geometries than established wire bonding and packaging techniques. To demonstrate the most basic scheme, we printed a collection of devices onto a thin, metal mesh on a transparent substrate, to form bottom contacts, and then established separate top contacts using a planar lithographic process (fig. S5). Figure 2, A and B, shows an exploded view schematic illustration and optical micrograph of an array of small, square devices (~25 μm by 25 μm), as well as those with shapes that spell "LED." The results indicate bright emission, even out to the edges of the devices, consistent with the relatively low surface recombination velocity in AlInGaP materials (*15*, *16*). For improved performance, ohmic contacts can be implemented by using established metallization and annealing schemes (*17*, *18*). One strategy involves additional processing on the source wafer to yield released devices with integrated ohmic contacts, suitable for printing and interconnection even on low-temperature substrates such as plastic or rubber. An alternative is to use low-temperature approaches to establish the ohmics directly on such substrates. For this work, we pursued the second strategy, using processes that involve temperatures below 175°C (see SOM for details and fig. S6 for transmission-line model analysis of the contact resistances). Figure 2C shows the layout of an ILED with ohmic contacts printed onto a thin layer of polyurethane on a glass substrate, and an optical micrograph of emission from a directly probed device. Figure 2, D and E, presents electrical and optical characteristics of a set of such devices, recorded on the wafer before undercut etching and after printing. The processing in this case used a passivation scheme to eliminate moderate degradation in performance associated with the HF etching step on unprotected devices (fig. S7). The resulting current-voltage-emission behavior of the printed devices is comparable to that of the devices on the wafer (see SOM for processing details and for statistics on devices with two different sizes).

Figure 3A provides a schematic illustration of an interconnect scheme for passive matrix addressing. Photolithography and electron beam evaporation define patterned metal electrodes [Ti (20 nm)/Au (300 nm)] that connect p and n contacts (nonohmic for the cases of Figs. 3 and 4) of devices in common columns and rows, respec-

tively. Two spin-cast, photopatterned layers of epoxy (1.2 μm thick) provide openings to these contacts; the top layer electrically separates the column and row electrodes at their crossing points. Connecting terminal pads at the ends of these electrode lines to external computer control systems via ribbon cables that use anisotropic conductive films (ACFs) enables passive matrix addressing (see SOM and fig. S8 for details). Figure 3B shows images of a small display that uses this design, formed on a thin sheet of plastic (PET, 50 μm thick) with a layer of a photocurable polyurethane as an adhesive. The ILEDs have dimensions of 100 μm by 100 μm and are configured into a 16 by 16 square array. The yields on the individual pixels for the case of Fig. 3B are 100%; at the level of the display, one column and two rows do not function, due to breaks in the contacts to the ACF ribbon cable [fig. S9; see SOM and fig. S10 for an example of similar display with even smaller ILEDs (50 μm by 50 μm)]. Such systems can be bent to radii of curvature of ~7 mm, with no observable degradation, even for several hundred cycles of bending (fig. S11). Analytical calculation shows that even at the minimum bend radius investigated here, the maximum strain in the ILED is 0.21%, with a somewhat smaller strain (0.19%) in the quantum well region (see SOM for details). Analysis using literature parameters to determine the dependence of the bandgap on strain (*19*–*22*) suggests changes in emission wavelength of ~2.4 nm for the smallest bend radius (see SOM for details).

As shown in Fig. 1, step-and-repeat printing can yield systems that cover areas much larger than those of the constituent ILEDs or the source wafer. One important outcome is the ability to form displays that can offer an effectively high level of transparency, where only the ILEDs (and the electrodes, if they are not made with transparent conductors) are opaque. Figure 3, C and D, shows examples of a 16 by 16 array, formed on glass. Here the area of the display is ~325 mm^2; the cumulative area of all the ILEDs is only ~2.5 mm^2, corresponding to less than ~1% of the display area. Figure 3C illustrates the operation of such a system positioned above a sheet of paper with printed logos; the focus of the image is on the paper, thereby illustrating a practical level of transparency for application in a heads-up display, for example. Figure 3D shows the same device (lower right), operating in front of a mirror (upper left) to demonstrate bidirectional emission characteristics. The inset provides a magnified view of a region of this display, in its off state to show the small sizes of the ILEDs compared to the unit cells. These layouts are critically important for many applications, due to the efficient utilization of the LED material, for reduced cost. For the examples shown, we achieved ~98% yields on the individual devices, and ~80% yields on the interconnections, limited by breaks in the metal lines and failed contacts to the ACF ribbon cable (fig. S12).

The devices and integration methods reported here are compatible with strategies to produce stretchable electronics (*12*, *13*), thereby providing a route to conformable displays and lighting systems of the type that might be interesting for integration with the human body and other curvilinear, deformable surfaces, all of which demand more than simple bending (e.g., Fig. 3B). Figure 4A shows an example of a stretchable ILED with the shape of a ribbon. This device was formed by transfer printing and bonding to a prestrained, rubber substrate of PDMS. Relaxing the prestrain creates a device with a "wavy," sinusoidal profile; this structure responds elastically to applied strain with a physics similar to that of an accordion bellows (*12*, *23*) to yield a stretchable ILED device. The top panels provide finite element simulation of the mechanics of the system in compressed (left) and stretched (right) configurations. The results indicate maximum strains in the ILED and the quantum well region of 0.36 and 0.053%, respectively (see SOM for details). The bottom panels show optical micrographs in the off (top) and on (bottom) states, with and without external illumination, respectively, in configurations similar to those illustrated in fig. S18A. The emission characteristics show no noticeable change in color with applied strain or associated changes in device geometry from "wavy" to flat (see SOM and figs. S13 and S14 for details). This observation is consistent with a calculated change in emission wavelength of less than ~0.7 nm based on our computed strain values and analysis similar to that performed for the flexible display (see SOM for details).

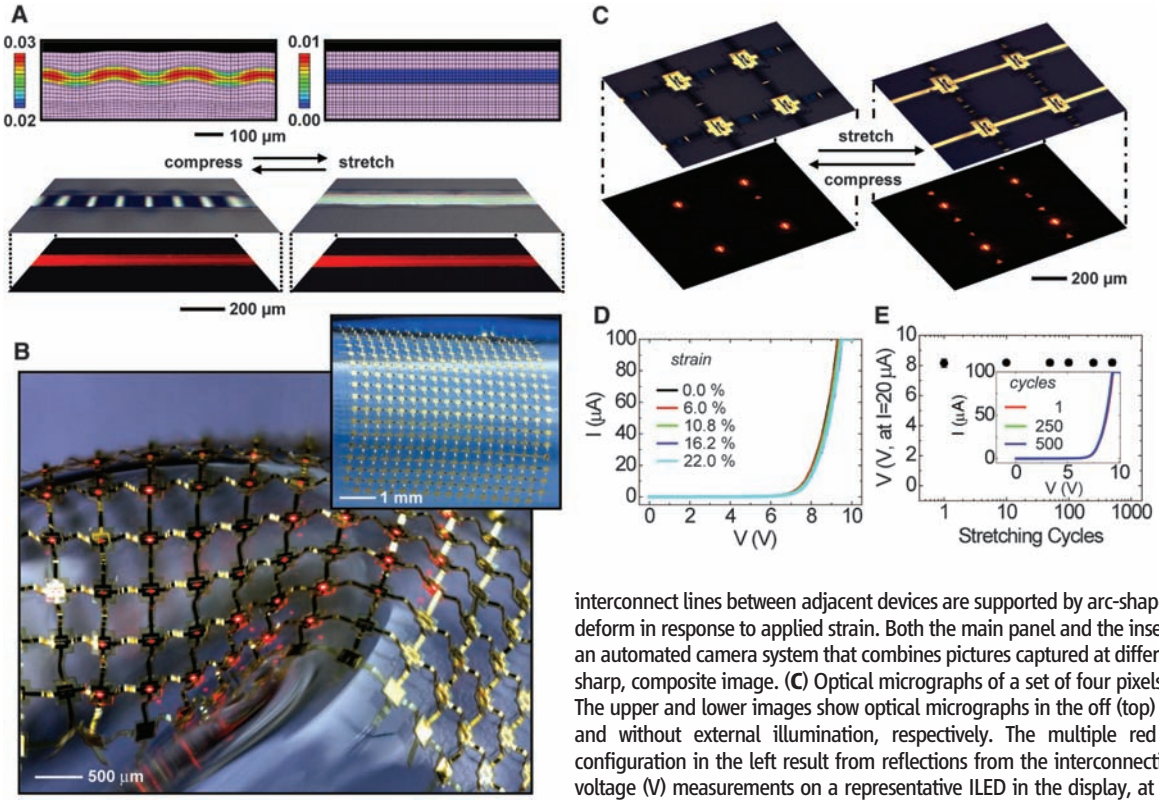

Fig. 4. (**A**) Color plots of the strain distributions (in percent) at the quantum well region and the corresponding finite element mesh used for simulation (top) and optical micrographs (bottom) of a stretchable ILED on a rubber substrate in unstrained and strained states. The bottom panels show optical micrographs in the off (top) and on (bottom) states, with and without external illumination, respectively. (**B**) Passive matrix, stretchable ILED display that uses a noncoplanar mesh configuration, on a rubber substrate. Here, interconnect lines between adjacent devices are supported by arc-shaped bridge structures that can deform in response to applied strain. Both the main panel and the inset images were collected with an automated camera system that combines pictures captured at different focal depths to provide a sharp, composite image. (**C**) Optical micrographs of a set of four pixels in the display shown in (B). The upper and lower images show optical micrographs in the off (top) and on (bottom) states, with and without external illumination, respectively. The multiple red spots in the case of the configuration in the left result from reflections from the interconnection bridges. (**D**) Current (I)–voltage (V) measurements on a representative ILED in the display, at different applied strains. (**E**) Voltage (V) needed to generate a current of 20 μA measured after stretching cycles to 500 times at an applied strain of 22%. The inset shows the *I-V* behavior after these cycling tests. These devices have relatively high turn-on voltages, due to the use of nonohmic contacts.

The "wavy" strategy of Fig. 4A can accommodate only a relatively modest range of applied strains (i.e., up to a few percent, for the designs reported here). A path to displays with high levels of stretchability uses non-coplanar mesh designs adapted from schemes reported for integrated circuits (*13*). Figure 4B presents optical micrographs of such a system, composed of a 16 by 16 square array of ILEDs bonded to a PDMS substrate and interconnected by electrodes supported by arc-shaped bridges, with a fraction of the pixels turned on (overall yield >80%) (see SOM and fig. S15 for details). The shapes of these bridges change in response to deformations of the display, in a way that isolates the ILEDs from any significant strains (figs. S16 and S17). In particular, calculation shows that for strains of 24%, as defined by the change in separation between inner edges of adjacent device islands, the maximum strains in the ILED and quantum well are only 0.17 and 0.026%, respectively. The computed change in emission wavelength is less than ~0.3 nm (see SOM for details). Figure 4C provides optical micrographs of four pixels in this display, in their off and on states, with (top) and without (bottom) external illumination, respectively, in compressed and stretched configurations. The images show the expected reduction in the heights of the arc-shaped bridges that lie in the direction of the applied tensile force (i.e., along the interconnects that run from lower left to upper right), together with an increase in the heights of the bridges in the orthogonal direction, due to the Poisson effect. This mechanical response is fully elastic—the bending-induced strains in the interconnects are small, the strains in the ILEDs are negligible, and the strain in the PDMS is well within its linear response regime. The data in Fig. 4, D and E, are consistent with this mechanics, as are the associated mechanics calculations. In particular, the current-voltage characteristics of a typical device do not change in a measurable way for applied strains up to ~22%, and we observe no degradation on cycling up to a few hundred times (500 times). Recent work demonstrates the use of smaller collections of large, conventional ILEDs in deformable devices that use different designs (*24*, *25*).

The schemes reported here for creating thin, small inorganic LEDs and for integrating them into display and lighting devices create design options that are unavailable with conventional procedures. The planar processing approaches for interconnect resemble those that are now used for organic devices and, for example, large-area electronics for liquid crystal displays, thereby conferring onto inorganic LED technologies many of the associated practical advantages. In large-area, high–pixel count systems (e.g., 1 million pixels per square meter), the ability to use LEDs with sizes much smaller than those of the individual pixels is critically important to achieve efficient utilization of the epitaxial semiconductor material, for reasonable cost. The minimum sizes of devices reported here are limited only by the resolution and registration associated with manual tools for photolithography.

References and Notes

1. S.-C. Lo, P. L. Burn, *Chem. Rev.* **107**, 1097 (2007).
2. F. So, J. Kido, P. Burrows, *MRS Bull.* **33**, 663 (2008).
3. D. A. Gaul, W. S. Rees Jr., *Adv. Mater.* **12**, 935 (2000).
4. S. Nakamura, G. Fasol, *The Blue Laser Diode: GaN Based Light Emitters and Lasers* (Springer, New York, 1997).
5. E. Yablonovitch, D. M. Hwang, T. J. Gmitter, L. T. Florez, J. P. Harbison, *Appl. Phys. Lett.* **56**, 2419 (1990).
6. H. X. Jiang, S. X. Jin, J. Li, J. Shakya, J. Y. Lin, *Appl. Phys. Lett.* **78**, 1303 (2001).
7. M. Konagai, M. Sugimoto, K. Takahashi, *J. Cryst. Growth* **45**, 277 (1978).
8. E. Yablonovitch, T. Gmitter, J. P. Harbison, R. Bhat, *Appl. Phys. Lett.* **51**, 2222 (1987).
9. C. Camperi-Ginestet, M. Hargis, N. Jokerst, M. Allen, *IEEE Trans. Photon. Tech. Lett.* **3**, 1123 (1991).
10. C. Carter-Coman, R. Bicknell-Tassius, A. S. Brown, N. M. Jokerst, *Appl. Phys. Lett.* **70**, 1754 (1997).
11. M. A. Meitl *et al.*, *Nat. Mater.* **5**, 33 (2006).
12. D. Y. Khang, H. Jiang, Y. Huang, J. A. Rogers, *Science* **311**, 208 (2006).
13. D.-H. Kim *et al.*, *Proc. Natl. Acad. Sci. U.S.A.* **105**, 18675 (2008).
14. J. Yoon *et al.*, *Nat. Mater.* **7**, 907 (2008).
15. M. Tamura *et al.*, *Jpn. J. Appl. Phys.* **37**, 3576 (1998).
16. E. F. Schubert, *Light-Emitting Diodes* P. 43, (Cambridge Univ. Press, Cambridge, UK, 2003).
17. C. L. Chen *et al.*, *Appl. Phys. Lett.* **48**, 535 (1986).
18. G. Stareev, *Appl. Phys. Lett.* **62**, 2801 (1993).
19. D. P. Bour *et al.*, *IEEE J. Quantum Electron.* **30**, 593 (1994).
20. F. H. Pollak, *Surf. Sci.* **37**, 863 (1973).
21. M. Chandrasekhar, F. H. Pollak, *Phys. Rev. B* **15**, 2127 (1977).
22. S. H. Pan *et al.*, *Phys. Rev. B* **38**, 3375 (1988).
23. H. Jiang *et al.*, *Proc. Natl. Acad. Sci. U.S.A.* **104**, 15607 (2007).
24. D. S. Gray, J. Tien, C. S. Chen, *Adv. Mater.* **16**, 393 (2004).
25. F. Axisa, F. Bossuyt, T. Vervust, J. Vanfleteren, *2nd Electronics System-integration Technology Conference (ESTC 2008)*, 1387, Greenwich, UK, 1 to 4 September 2008.

26. We thank T. Banks for help with processing using facilities at the Frederick Seitz Materials Research Laboratory; S. Mikael, V. Malyarchuk, H. C. Ko, and S.-G. Koo for assistance with display operating interface; J. D. Sulkin for help with current-voltage-emission measurement; A. P. Le for help with measurement of emission spectra; and C. Conway, Z. Johnson, and H.-S. Kim for help with photography. This material is based on work supported by Ford Motor Company, the NSF (grant DMI-0328162), and the U.S. Department of Energy, Division of Materials Sciences (Award No. DE-FG02-07ER46471), through the Materials Research Laboratory and Center for Microanalysis of Materials (DE-FG02-07ER46453) at the University of Illinois at Urbana-Champaign. S.-I. Park and R.-H. Kim thank Samsung for doctoral fellowships.

Supporting Online Material

www.sciencemag.org/cgi/content/full/325/5943/977/DC1
Materials and Methods
Figs. S1 to S19
References

1 May 2009; accepted 1 July 2009
10.1126/science.1175690

Visualization of Fermi's Golden Rule Through Imaging of Light Emission from Atomic Silver Chains

Chi Chen,[1] C. A. Bobisch,[2] W. Ho[1,2]*

Atomic-scale spatial imaging of one-dimensional chains of silver atoms allows Fermi's golden rule, a fundamental principle governing optical transitions, to be visualized. We used a scanning tunneling microscope (STM) to assemble a silver atom chain on a nickel-aluminum alloy surface. Photon emission was induced with electrons from the tip of the STM. The emission was spatially resolved with subnanometer resolution by changing the tip position along the chain. The number and positions of the emission maxima in the photon images match those of the nodes in the differential conductance images of particle-in-a-box states. This surprising correlation between the emission maxima and nodes in the density of states is a manifestation of Fermi's golden rule in real space for radiative transitions and provides an understanding of the mechanism of STM-induced light emission.

The scanning tunneling microscope (STM), which is based on the tunneling effect, has been used to visualize various quantum phenomena in real space, including the quantum corral (*1*), quantum mirage (*2*), and particle-in-a-box states (*3*, *4*). All of these demonstrations involved the localization of the electron density of states in confined nanostructures. Light emission from the STM junction reveals a different kind of quantum phenomenon that involves the optical transitions and inelastic electron tunneling (IET) processes in single molecules (*5*, *6*) and nanostructures (*7*). Furthermore, photon intensity imaging with atomic resolution has been demonstrated (*8*–*10*). The spatial resolution in these optical experiments originates from the precision of the STM in injecting electrons in a confined space, although the emitted photons are collected in the far field. This atomic-scale optical detection can reveal aspects of the molecules and nanostructures that are hidden when probed with other techniques.

Imaging of STM light emission has not yet been directly correlated with the underlying elec-

[1]Department of Chemistry, University of California, Irvine, CA 92697, USA. [2]Department of Physics and Astronomy, University of California, Irvine, CA 92697, USA.

*To whom correspondence should be addressed. E-mail: wilsonho@uci.edu